A Novel Zinc Complex with Ethylenediamine Schiff Base for Highly Luminance Blue Fluorescent OLED Applications

Alexey N. Gusev,[a]* Mikhail A. Kiskin,[a] Elena V. Braga,[a] Marian Chapran,[b] Gabriela Wiosna-Salyga,[b] Gleb V. Baryshnikov,[c,d] Valentina A. Minaeva,[e] Boris F. Minaev,[e] Khrystyna Ivaniuk,[f] Pavlo Stakhira,[f] Hans Ågren,[c,d] and Wolfgang Linert[g]

[a] *N.S. Kurnakov Institute of General and Inorganic Chemistry, Russian Academy of Sciences, Moscow, 119991, Russia. galex0330@gmail.com*

[b] *Department of Molecular Physics, Lodz University of Technology, Zeromskiego 116, 90-924, Lodz, Poland*

[c] *Division of Theoretical Chemistry and Biology, School of Engineering Sciences in Chemistry, Biotechnology and Health, KTH Royal Institute of Technology, 10691, Stockholm, Sweden*

[d] *Tomsk State University, 36 Lenin Avenue, Tomsk, Russia*

[e] *Department of Chemistry and Nanomaterials Science, Bohdan Khmelnytsky National University, 18031, Cherkasy, Ukraine*

[f] *Lviv Polytechnic National University, Stepan Bandera 12, 79013, Lviv, Ukraine*

[g] *Institute of Applied Synthetic Chemistry, Vienna University of Technology, Getreidemarkt 9/163-AC, A-1060 Vienna, Austria.*

Abstract

To explore the photophysical properties of coordination compounds with bright blue fluorescence an azomethin-zinc complex was synthesized and characterized by various techniques (EA, TG, IR- mass-spectroscopy). The crystal structure was determined by X-ray diffraction analysis. Through thermal characterization this complex was proved to have good thermal stability. Photoluminescence spectra were

recorded both in solution and in the solid state, and the complexes showed noteworthy photoluminescence with a maximum in the blue region. The results of time-dependent density functional theory calculations indicated that the origin of luminescence for the title complex is due to a combination of monomer and eximer emissions. The light emission performance of the zinc complex in organic light emitting diodes (OLEDs) was investigated, and the results indicated superior electroluminescnce properties as a blue fluorescent light source (max. brightness 17 000 cd/m^2, max. EQE = 5%).

Place for grafical abstract

1. INTRODUCTION

The synthesis and development of new electroactive emitters for high performance organic light emitting diodes (OLEDs) is one of the key problems of modern materials science. It is well-known that a general target for OLED investigations is to develop full-colour displays and solid state lighting (SSL) sources. Despite the significant progress achieved in this field in the last decade, the production of blue monochromatic materials that can be used as active emissive layers in OLEDs remains an important problem that so far as hampered the production of a complete white electroluminescence involving a balanced simultaneous emission of the three primary colours of light.[1-5] The implementation of such blue emitters in displays and SSL technologies are limited due to low lifetime and a high roll-off efficiency in the electroluminescent devices.[6-8] Moreover, wide electroluminescence spectra of such materials frequently do not meet the requirements of colour purity.[9] Among the most

promising organic emitters that demonstrate state-of-art lighting characteristics within deep-blue fluorescent OLEDs one can mention the Lee's naphthyl-linked phenanthroimidazole–carbazole hybrid species (external quantum efficiency EQE_{max}=6.6%),[10] C6- and C9-substituted phenanthro[9,10-d]imidazoles (EQE_{max}=5.8%)[11] and 1,2-bis(4'-(1-phenyl-1-H-benzo[d]imidazol-2-yl)-[1,1'-biphenyl]-4-yl)-1H-phenanthro[9,10-d] imidazole (EQE=4.1%),[12] Jayabharathi's twisted dihydrobenzodioxin phenanthroimidazole derivatives (EQE_{max}=5.3%),[13] Yang's *meta*-linked donor–acceptor triphenylamine-phenanthroimidazole species (EQE_{max}=3.3%)[14] and 4-[2-(4′-diphenylamino-biphenyl-4-yl)-phenanthro[9,10-d]imidazol-1-yl]-benzonitrile (EQE_{max}=7.8%).[15] Very recently, S. K. Pal et al.[16,17] have published very interesting utilization of room-temperature columnar pure organic liquid crystals for the fabrication of blue OLEDs with and highest EQE of 4.0%.

Luminescent metal-organic compounds containing functional emissive ligands represent an emerging class of luminescent materials because they possess the advantages of both organic dyes (tunable and intense emission), and transition-metal based emitters (high photostability and large Stokes shifts).[18-21]

The interest in Zn(II) complexes with Schiff bases has been recently boosted due to their strong photoluminescence emissions. However, organic electroluminescent devices with a high luminance of ~ 1000 cd m^{-2} and photostability were reported only through use of a limited number of Zn(II) complexes.[18-21] Among different classes of zinc(II) complexes, which are of interest as "low-cost" electroluminescent materials, complexes based on N,N-bis(salicylidene)ethylenediamine ligands are of special interest because these systems exhibit intense luminescence in the blue region of the

visible spectrum. Moreover, their straightforward synthesis makes available a wide selection of ligands, which differ from each other with regards to the nature of the diamine moiety or with the substituents placed on the salicylidene core and which makes it possible to fine-tune the emission properties. Studies of correlations between the composition, structure, and functional properties (luminescence, thermal stability, volatility, conductivity, etc.) of starting complexes have thus underlined the design of new electroluminescent materials.[22-28]

Ethylenediamine Schiff base of 4-acylpyrazolone derivatives can provide a structural and functional analogue of Salen-type systems (Scheme 1). In this way, it is possible to obtain due to their basis fluorescent materials with the desired properties. At the same time, only few studies of the photo- and electroluminescent properties of Zn complexes with such ligands have been described in the literature up to date.[29,30] Based on the above considerations, we focus in this paper on syntheses, structures and luminescent properties of new zinc(II) coordination compounds based on N,N'-ethylamine-bis[1-phenyl-3-methyl-4-formylimino-2-pyrazoline-5-ol] (H_2L) and evaluate them as blue emitters in OLEDs.

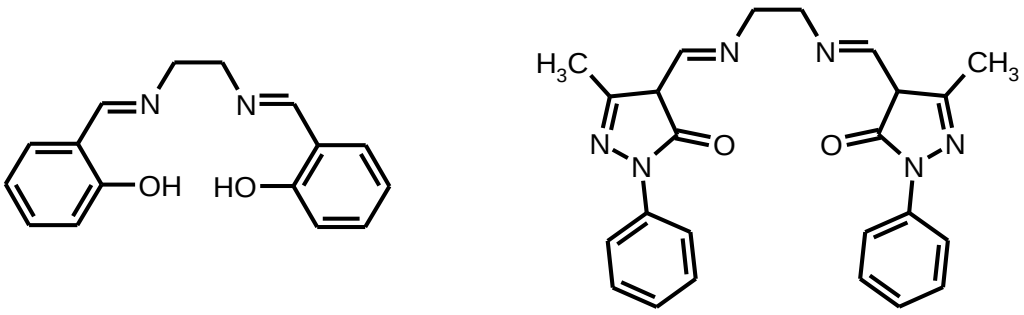

H_2Salen H_2L

Scheme 1. The structure of protonated Salen ligand (left) and its modified analogue (right) prepared in this work.

2. EXPERIMENT

2.1. Materials and methods. All starting reagents and chemicals were purchased from Aldrich or Merck and were used without further purification. The 3-methyl-1-phenyl-4-formylpyrazol-5-ol ligand was synthesized as described in the literature.[31] High-purity solvents for spectroscopic studies were obtained from the Aldrich company. Elemental analyses of C, H, and N were performed with an EuroEA 3000 analyzer. Absorption spectra were recorded with a Carry 5000 (Varian) spectrometer. Photoluminescence spectra of solutions, thin films and solid state samples were recorded on FluoroMax-4 and Edinburgh Instruments FLS980 fluorescence spectrometers. The quantum yields of the solid samples were determined under ligand excitation by the absolute method using an integrating sphere. The fluorescence quantum yield of the compound was determined in 100 μM solution by comparison with the fluorescence of quinine sulfate in 0.1 M sulfuric acid ($\varphi = 0.55$), taken as a reference fluorescence standard.[32,33] The IR spectra were measured by the FSM 2202 spectrometer with KBr pellets in the range 4000-400 cm^{-1}. Electrospray mass spectra of complex were measured with a Finnagan TSQ 700 mass spectrometer in positive ion mode. Samples were prepared at a concentration of ~2 mg/ml MeOH. The mass spectra were acquired over the m/z range of 50-2000; several scans were averaged to provide the final spectrum. Thermogravimetric experiments were performed using the Paulik-Paulik-Erdey Q-derivatograph under a static air atmosphere. Devices. OLEDs have been fabricated on pre-cleaned, patterned indium-tin-oxide (ITO) (100 nm) coated glass

substrates obtained from Ossila. All organic semiconductors and cathode layers were thermally evaporated under pressure of 10^{-5} mbar in physical vapour deposition system. The size of the pixels was 6 mm^2. Calcium and aluminium were used as the cathode. Output characteristics of the OLEDs were measured using a semiconductor parameter analyzer HP4145A. The measurement of brightness was obtained using a calibrated photodiode[34] and the electroluminescence spectra were recorded with an Ocean Optics USB2000 spectrometer.

2.2. Synthesis of the zinc complex. 1,2-Ethylenediamine (120 mg, 2 mmol) was added dropwise during 10 min to a 30 ml ethanol solution of 4-methyl-1-phenyl-4-formylpyrazol-5-one (808 mg, 4 mmol). The resulting mixture was stirred and heated at reflux for 1 h. After this zinc acetate dehydrate (438 mg, 2 mmol) was added and the reaction mixture was continually heated under reflux for 2 h. The resulting solution was cooled to room temperature. White precipitate was filtered and washed with EtOH (2 x 5 mL). The washed product was recrystallized in methanol to give the complex 1 as colorless fine crystals. (Yield: 522 mg (51%) base on 1,2-ethylenediamine). Anal. Calcd. for $C_{24}H_{24}N_6O_3Zn$: C, 56.53; H, 4.74 %; N, 16.48 %. Found: C, 56.61; H, 4.41, N, 16.23. FT-IR (KBr), cm^{-1}: 1634 (s), 1597(m), 1527(m), 1502(s), 1335(s), 755(s), 688(m), 608(m), 440 (m). ^1H NMR (400.1 MHz, $(CD_3)_2SO$, ppm) δ 8.34 (s, 1H), 8.17 (d, 2H), 7.42 (d, 2H), 7.16 (d, 1H), 3.62 (s, 2H), 2.21 (s, 3H). ESI-MS (positive) in methanol: the base peak was detected at m/z = 491.11 corresponding to the $[Zn(L)+H]^+$ species.

2.3. Crystallography. Single crystal X–ray diffraction data were collected using the Bruker APEX II diffractometer equipped with a CCD detector and a graphite-

monochromated MoKα radiation source (λ = 0.71073 Å) at the User Facilitiy Centers of the Kurnakov Institute of General and Inorganic Chemistry. The structures of complexes were solved by the direct methods and refined in the full-matrix anisotropic approximation for all non–hydrogen atoms. The hydrogen atoms of water molecule were found in differential Fourier maps and their parameters were refined using the riding model. The hydrogen atoms of the carbon-containing ligand were positioned geometrically and refined by using a riding model. All the calculations were performed by direct methods and using the SHELX–2014 program package.[35,36] The crystallographic parameters and the structure refinement statistics for 1 at T = 100(2) K are as follows: $C_{24}H_{24}N_6O_3Zn$, M_w = 509.86, block colorless crystals, 0.20 x 0.10 x 0.10 mm, space group $P2_1/c$, a = 12.3633(9) Å, b = 17.1509(13) Å, c = 10.8510(8) Å, β = 100.6560(10)°, V = 2261.2(3) $Å^3$, Z = 4, d_{calc} = 1.498 g cm^{-3}, μ = 1.126 mm^{-1}, 2.05 ≤ θ ≤ 30.54, 22074 measured reflections, 5364 reflections with I > 2σ(I), R_{int} = 0.058, GOOF = 0.897, R_1 (I > 2σ(I)) = 0.033, wR_2 (I > 2 σ(I)) = 0.082, R_1 (all data) = 0.047, wR_2 (all data) = 0.087. More detail can be found in CCDC 1896280.

3. COMPUTATIONAL DETAILS

The structures of the [ZnL] the complex with and without solvated water molecule were optimized by the B3LYP/6-31G(d)[37-40] method in a vacuum approximation. For the optimized structures the vertical absorption spectra were calculated by the same B3LYP/6-31G(d) technique within the time-dependent (TD) DFT[41] approximation accounting also for solvent effects through the polarized-continuum model (PCM).[42] The same TD DFT level of theory was used for the

optimizing of $([ZnL])_2$ dimers is the first singlet excited state (excimer model). Bader's QTAIM analysis[43] for the fragment of crystal packing $([ZnL]\cdot H_2O)_3$ was carried out based on the obtained X-ray geometries in order to take the crystal packing effect into account in an implicit way. The energies of coordination, hydrogen bonds and other non-covalent bonds (E_{bond}) have been estimated by the simple Espinosa-Molins-Lecomte (EML) relationship[44,45]:

$$E_{bond} = 0.5\, v(\mathbf{r}),$$

where ν(r) is the potential energy density value (negative by definition) in the corresponding bond critical point (CP) of the (3, -1) Bader's type.[43] The DFT and TDDFT calculations were performed using the GAUSSIAN 16 software,[46] while the QTAIM computations where carried out within the AIMAll program package.[47]

4. RESULTS AND DISCUSSION

4.1. IR, TGA and single-crystal X-ray characterization of complex 1. The zinc complex **1** was obtained by reaction of 1 equivalent of ligand H_2L with $Zn(OAc)_2$ in ethanol. The product was isolated from the reaction solution by slow crystallization. After recrystallization, filtration, followed by washing with cold methanol resulted in the production of crude products with moderate yields. The formation of metal complex **1** was confirmed by means of the ESI mass spectrometry and elemental analyses.

The IR-data confirmed that the H_2L organic species acts as a dinegative tetradentate ligand forming a conjugated chelate ring in the enolized form in their Zn(II) complex. The IR spectra of the complex demonstrate disappearance of the NH and C=O bands. The B3LYP/6-31G(d) calculations are in a good general agreement with the

observed IR spectrum (Figure S1, Table S1). After geometry optimization of the studied complex by the DFT method we obtained the complete set of real vibration frequencies and made a reliable assignment of all observed IR absorption bands (Figure S1). In the IR spectrum of the complex the complicated intense band at 1634 cm^{-1} with a weak shoulder 1655 cm^{-1} are assigned to the azomethine C=N stretching (out-of-phase) vibrations of the Schiff-base and to the C–O (in-phase) stretching vibrations, respectively. We have to note that the water molecule H–O_3–H bending vibration provides also a significant contribution to the 1634 cm^{-1} band. The aromatic C=C stretching vibrations in the phenyl (ph) moieties are found at 1597 cm^{-1}. The O–C=C–CH stretching vibrations and pyrazoline ring C=N stretching frequency are indentified with the band 1527 cm^{-1}. The close-lying intense absorption band at 1502 cm^{-1} is assigned to the asymmetric C=C stretching vibrations of the phenyl rings and to C(ph)–N1(N6) stretching vibrations. The intense absorption features at 608, 466, 440 cm^{-1} have large contributions from the stretching vibrations of the coordination bonds Zn–N and Zn–O[48] (Figure S1).

A thermogravimetric analysis (TGA) was performed on the polycrystalline sample of the complex in air atmospheres and the TGA curve is shown in Fig. S2. Compound **1** is very stable upon heating and started to lose weight only up to 153 ^oC. This is the part of 3.39% of its weight, being approximately equal to the weight percentage of the coordination water molecule in the [ZnL]·H_2O complex (calc.: 3.52%). We fixed the desolvation process accompanied by the endothermic effect (ΔH = 52.4 kJ/mol) with a maximum at 183.7^oC. The unhydrated sample is stable till to 334 ^oC. Heating the sample to higher temperatures led to decomposition of the organic

components. The overall weight loss at temperature up to 550 °C of 84.3% matches the calculated value (84.14%) assuming that the residue is ZnO.

The molecular structure of the complex deduced from X-ray diffraction analysis is shown in Figure. 1. The complex **1** is a neutral, mononuclear, molecule with the Zn ion being pentacoordinated by the deprotonated H_2L ligand, where in addition to the N_2O_2 donor set provided by the tetradentate Schiff base ligand, a water molecule is coordinated to the Zn(II) center. The coordination polyhedron around the metal center is best described as a distorted square pyramidal with Addison's parameter 0.41.[49] Zn atom deviation from the pyramid base plane (O1N3N4O2) is 0.3598(6) Å. The Zn–O bond lengths of 2.025 and 2.002 Å from the Schiff base ligand and 2.056 Å from water molecule are slightly longer than those documented in the literature, whereas the Zn–N bond lengths of 2.065 and 2.087 Å are also slightly longer than the literature values.[29,30] In addition, the bond lengths of O1–C7 (1.280(2) Å), O2–C18 (1.278(2) Å) demonstrate that the oxygen (O1 and O2) of the carbonyl groups takes part in the coordination by the enolic form, and their active hydrogen is replaced by the Zn(II) ion. Both phenylpyrazolate arms are probably planar, the angles between the mean planes are 0.8° and 8.4°, respectively. DFT optimization supports these experimental findings in many details. The main conclusion concerns the fact that both DFT and X-ray analysis provide an asymmetric and non-planar structure of complex **1**.

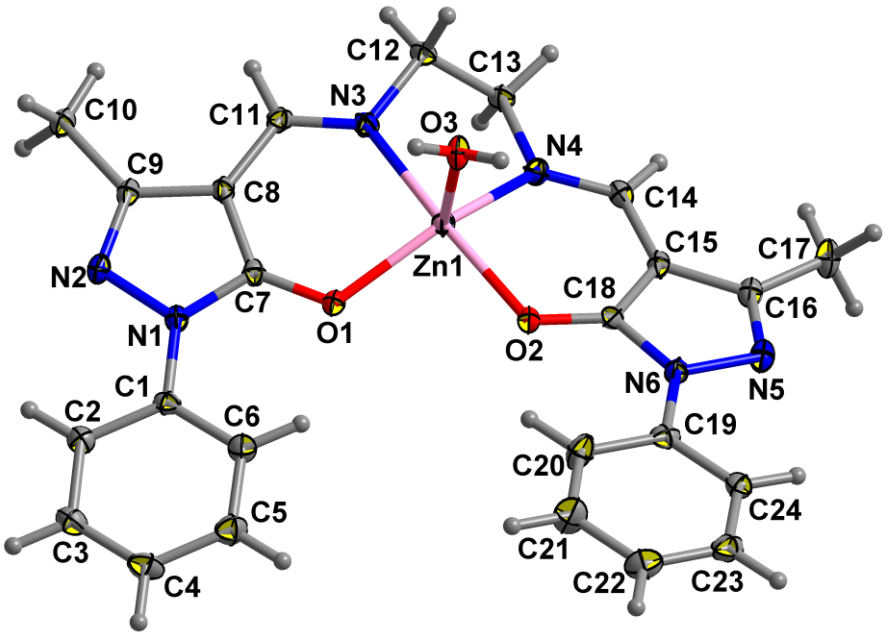

Figure 1. Structure of complex **1** (thermal ellipsoids are shown with probability 50%). Selected bond lengths (Å) and bond angles (deg) are: Zn1-O2 2.0024(13), Zn1-O1 2.0263(13), Zn1- Zn1-O3 2.057(2), Zn1-N3 2.065(2), Zn1-N4 2.087(2), O2-Zn1-O1 92.74(5), O2-Zn1-N3 170.45(6), O1-Zn1-N3 91.41(6), O2-Zn1-O3 93.07(6), O1-Zn1-O3 106.20(6), O3-Zn1-N3 94.02(6), O2-Zn1-N4 91.99(6), O1-Zn1-N4 145.55(6), N3-Zn1-N4 79.77(6), O3-Zn1-N4 107.59(6).

The crystal packing of complex **1** is stabilized by means of hydrogen bonding and π–π stacking interactions. Intermolecular H-bonds (O3–H3C···N2a: O-H 0.80 Å, O···N 2.746(2) Å, H···N 2.07 Å, O-H-N 168.3º: O3-H3C···N5b: O-H 0.76 Å, O···N 2.857(2) Å, H···N 2.00 Å, O-H-N 166.6º) between the coordinated water molecules and N atoms of pyrazolone rings in the ligand anion from neighboring complex molecules form a 1D network (Figure 2).

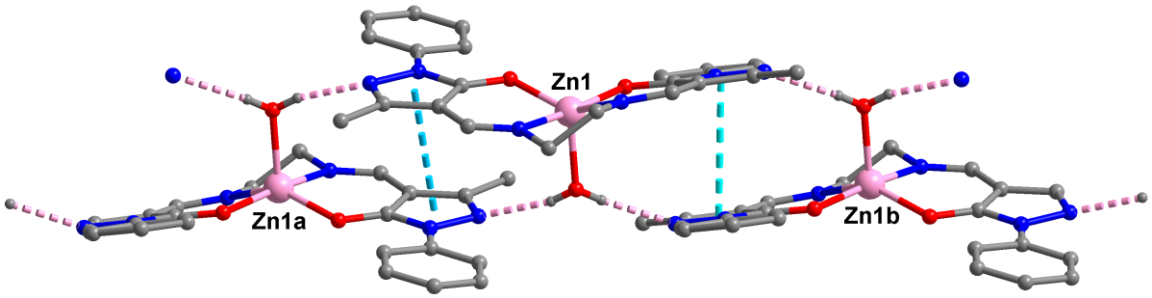

a

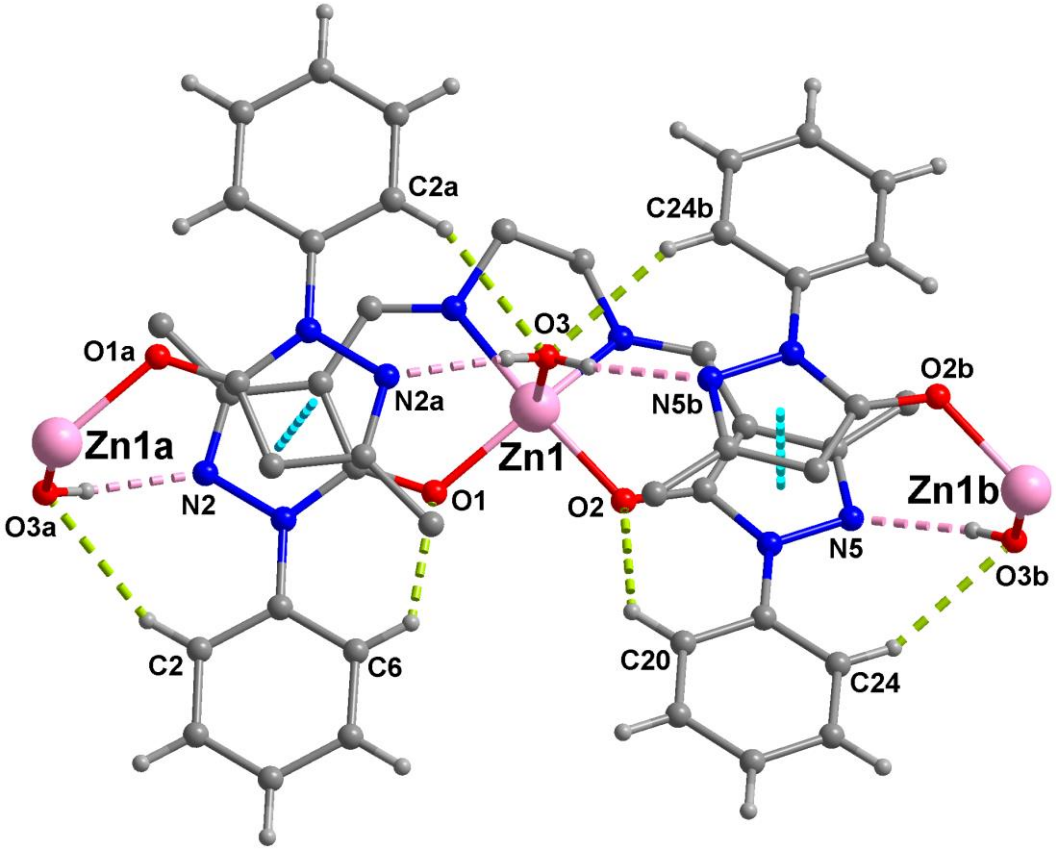

b

Figure 2. The 1D network of complex 1: a) side view, b) top view. Dotted lines represent the O–H···N, CH···O and π–π interactions (symmetry codes: (a) 1-x, -y, 1-z, (b) 2-x, -y, 2-z). CH···O interactions parameters: C2a–H···O3, C···O 3.406 Å, H···O 2.61 Å, C-H-O 141.1º; C6-H···O1, C···O 2.887 Å, H···O 2.23 Å, C-H-O 125.2º; C20-H···O2, C···O 2.824 Å, H···O 2.15 Å, C-H-O 126.5º; C24b-H···O3, C···O 3.327 Å, H···O 2.48 Å, C-H-O 147.9º.

As shown in Figure 2, the hydrogen bonded supramolecular network is further supported by π–π stacking interactions, in which the centroid-to-centroid separations of

two pyrazole rings are found to be 3.43 and 3.80 Å. The energy of desolavation obtained from TGA analysis (+52.4 kJ/mol or +12.5 kcal/mol, where plus means here that energy is spent for the bond breaking) is almost four times smaller than the total EML energy[44,45] (-49 kcal/mol, minus means that energy is released upon the bond formation) of one Zn-O3 bond and of the four hydrogen bonds which bind each H_2O molecule with two neighboring [ZnL] molecules (Figure 2b, Table 1). Such overestimation is a known limitation of the EML relationship,[50] while the direct estimation of the Zn-O_3 bond energy $E_{bind.} = (E_0+E_{ZPE})_{[ZnL]\cdot H2O} - (E_0+E_{ZPE})_{[ZnL]} - (E_0+E_{ZPE})_{H2O}$ provides a more reliable value -12.3 kcal/mol (herein E_0 corresponds to the energy of optimized structure, E_{ZPE} is a zero-point energy value) in excellent agreement with dehydration energy (-9.6 kcal/mol) for the related [Zn(salen)]·H_2O complex calculated by Vladimirova et. al.[51] However, DFT optimization for the isolated [ZnL]·H_2O cluster results in a significantly elongated Zn-O_3 distance (2.184 Å vs. 2.057 Å from X-ray data) that is reasonably correspond to the weakened Zn-O_3 bond comparing with the EML scheme.

Thus, we can conclude that the calculated absolute EML energies for the non-covalent and coordination bonds of the studied system are slightly underestimated, but that they still demonstrate the correct view on the relative energies of these bonds. In fact, as can be seen from the Bader's QTAIM analysis (Table 1) the bonds O3···HC are not strictly equivalent by electronic characteristics and they are three times weaker than the O3H···N2 bonds. Both O3···HC ([ZnL] (1a)) and O3···HC ([ZnL] (1b)) bonds demonstrate high values of elipticity (ε = 0.2 and 0.98 respectively) indicating high dynamic instability.[43]

Table 1. Topological characteristics of the Zn-O and Zn-N coordination bonds and hydrogen bonds responsible for the binding of water in the crystal packing fragment ([ZnL]·H_2O)

Bonds	*d*, Å	$\rho(\mathbf{r})$, $e \cdot a_o^{-3}$ *	$v(\mathbf{r})$, a.u.	$g(\mathbf{r})$, a.u.	$h_e(\mathbf{r})$, a.u.	$\nabla^2\rho(\mathbf{r})$, $e \cdot a_o^{-5}$	ε	E (EML) kcal mol^{-1}
Zn1–O3 [ZnL] (1)	2.057	0.0653	-0.1052	0.0881	-0.0170	0.2846	0.07	-33.0
Zn1-O1 [ZnL] (1)	2.025	0.0736	-0.1207	0.0977	-0.0231	0.2984	0.07	-37.9
Zn1-N4 [ZnL] (1)	2.088	0.0742	-0.1123	0.0858	-0.0265	0.2376	0.09	-35.2
Zn1-O2 [ZnL] (1)	2.002	0.0782	-0.1311	0.1050	-0.0261	0.3157	0.03	-41.1
Zn1-N3 [ZnL] (1)	2.064	0.0793	-0.1230	0.0924	-0.0306	0.2471	0.05	-38.6
O3··· HC [ZnL] (1a)	2.481	0.0088	-0.0062	0.0074	0.0012	0.0347	0.20	-2.0
O3··· HC [ZnL] (1b)	2.614	0.0067	-0.0044	0.0058	0.0014	0.0291	0.98	-1.4
O3H··· N2 [ZnL] (1a)	2.071	0.0230	-0.0189	0.0191	0.0002	0.0772	0.06	-5.9
O3H··· N5 [ZnL] (1b)	2.047	0.0242	-0.0214	0.0222	0.0008	0.0917	0.06	-6.7

All the O3···HC and O3H···N2 bonds correspond to the closed-shell type interactions ($h_e(\mathbf{r}) > 0$, $\nabla^2\rho(\mathbf{r}) > 0$ in the corresponding (3, -1) CPs) as well as other numerous intermolecular and intramolecular π-π stacking interactions that couple [ZnL] complexes within the crystal packing (Tables S1, S2 and Figure S1). The calculated Laplacian values and electron density $\rho(\mathbf{r})$ values (Tables 1, S1, S2) for most of non-covalent inter- and intramolecular hydrogen bonds and Van der Waals interactions coincide with the Koch-Popelier average range for a large number of the hydrogen bond examples (0.024–0.139 ea_0^5 and 0.002–0.035 ea_0^3, respectively).[52] The remaining part of the non-covalent bonds that do not satisfy the Koch-Popelier criteria are characterized by very small values of the Laplacian, electron density and potential energy density $v(\mathbf{r})$ in the corresponding (3, -1) critical points. Together with the high elipticity this

indicates the existence of these bonds only upon fixed positions of the atomic nuclei. In fact, these bonds are only statically stable, but in a real crystal they do not exist.

All the coordination bonds Zn-N and Zn-O are characterized by positive values of the electron density Laplacian and by negative electron energy density $h_e(\mathbf{r})$ values. From one side, the positive Laplacian values indicate an outflow of electron density from interatomic space into the atomic basins of the Zn and N,O atoms; but from another point of view the negative $h_e(\mathbf{r})$ values mean that the potential energy density $v(\mathbf{r})$ in the corresponding critical point of the Zn–N and Zn–O bonds dominates over the kinetic energy density, $g(\mathbf{r})$. Both these facts specify the Zn–N and Zn–O coordination bonds as intermediate type interactions between the covalent (shared) and non-covalent (closed-shell) contacts similar to other DFT studied Zn complexes with Schiff bases.[53-57]

4.2. Absorption spectra. The absorption spectra of the anhydrous [ZnL] complex measured in different solvents and thin film demonstrate the same position of the first absorption maximum at around 336 nm (Figure 3a). We have not found a clear dependence of the first absorption band position on the polarity of the solvent; however, the shape of the remaining part of absorption spectra is quite different in polar (THF, ethanol, acetonitrile) and non-polar ($CHCl_3$) media. The most probable explanation is that in the polar media the hydrous complex can dissociate and thus the S_1 and S_2 states of become degenerated for [ZnL] complex, while in the $CHCl_3$ non polar solvent as well as in the solid film H_2O molecule still coupled to the complex providing the splitting of S_1 and S_2 states on about 0.11 eV for $[ZnL]\cdot H_2O$ complex. As follows from our TD DFT calculations the first absorption maximum around 330 nm (Fig. 3) corresponds to the quasi-degenerate S_0-S_1 and S_0-S_2 transitions (calc.: 309-315 nm for

different solvents). Such degeneracy of the S_1 and S_2 states is caused by the formal dimeric structure of the H_2L ligand in which the chromospheres are separated by the ethylamine spacer. As a result, the HOMO and HOMO-1 orbitals of the anhydrous [ZnL] complex are almost equivalent (-5.59 and -5.60 eV, respectively, Figure 3b); thus, the S_0-S_1 and S_0-S_2 transitions lie close in energy corresponding to the HOMO-1 → LUMO and HOMO → LUMO excitations (Figure 3b). When the H_2O molecule is coordinated to the Zn atom the HOMO and HOMO-1 become slightly non-equivalent (-5.44 and -5.55 eV, respectively, Figure 3b) that provides the splitting of the S_1 and S_2 states on about 0.15 eV (Table 2).

The calculated intensity of both S_0-S_1 and S_0-S_2 transitions is rather limited because of the charge-transfer (CT) character of the corresponding excitations (Figure 3b). The first transition is more intense since it does not include much destructive interference from additional excitations. It is important to note that there is no significant contribution of the Zn *d*-atomic orbitals into the HOMO-1, HOMO and LUMO wave functions which indicates only a complexing role of the Zn^{2+} ion. Thus, it cannot serve as a heavy atom and induce spin-orbit coupling effect on the singlet-triplet intersystem crossing.[58,59] Actually, complexation of the H_2L ligand with the Zn^{2+} complex provides the significant stability increase of the organic chromospheres together with the increased molecular rigidity that affects the suppressing of non-radiative quenching channels.

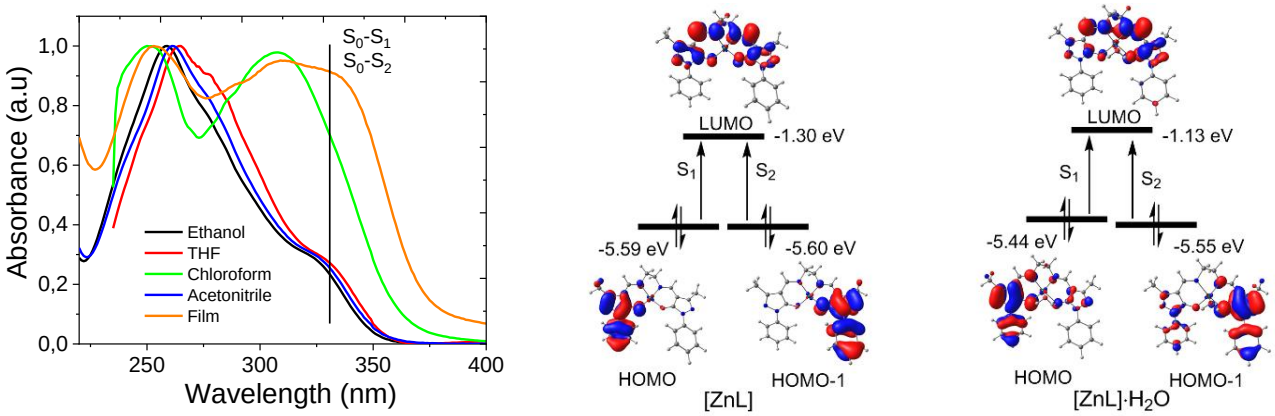

a *b*

Figure 3. (a) Normalized absorption spectra of the dilute solutions (10^{-5} M in chloroform, THF, ethanol, acetonitrile) and for the thin solid film of the [ZnL] complex; (b) orbital diagram for the [ZnL] and [ZnL]·H_2O complexes calculated by the B3LYP/6-31G(d) method.

Table 2. The characterization of the S_1 and S_2 excited singlet states for the [ZnL] and [ZnL]·H_2O isolated complexes calculated by the B3LYP/6-31G(d) method within TD DFT approximation. Experimental wavelengths are given in parenthesis.

Solvent	State	[ZnL]			[ZnL]·H_2O		
		λ_{abs}, nm	*f*	Assignment	λ_{abs}, nm	*f*	Assignment
THF	S_1	313 (330)	0.064	HOMO → LUMO (96%)	316	0.072	HOMO → LUMO (97%)
	S_2	312	0.006	HOMO-1 → LUMO (91%)	306	0.004	HOMO-1 → LUMO (90%)
$CHCl_3$	S_1	315	0.043	HOMO → LUMO (95%)	317	0.066	HOMO → LUMO (97%)
	S_2	314	0.004	HOMO-1 → LUMO (93%)	308	0.003	HOMO-1 → LUMO (91%)

4.3. Luminescence spectra. The photoluminescence behaviour of the zinc complex, examined in EtOH, $CHCl_3$, CH_3CN, THF media at room temperature (298 K), are presented in Figure 4. Selected data are summarized in Table 3.

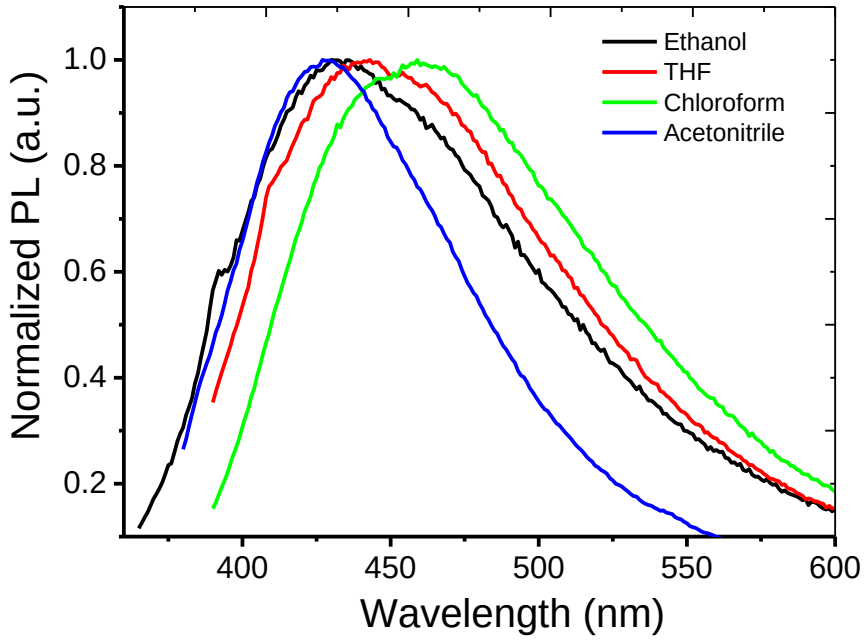

Figure 4. Normalized emission spectra of [ZnL] complex in different solvents.

Upon irradiation of ultraviolet light by a wavelength corresponding to the maximum in the excitation spectrum (345-370 nm) we have observed quite weak blue fluorescence with a maximum wavelength varying in the range 430-460 nm depending on the solvent polarity. In the more polar CH_3CN solvent the [ZnL] complex demonstrated more deep blue emission at 429 nm with higher quantum yield (0.19) comparing with the chloroform solution (460 nm vs. QY = 9.1%). The photoluminescence lifetimes measured at the emission maxima wavelength are ranged in the nanosecond scale (Table 3) proving the fluorescence nature of the luminescence and the absence of the heavy atom effect from the metal.[58]

As mentioned above, we have predicted the potential application of the studied zinc complexes as a promising emissive material for OLED applications. Therefore, the solid-state fluorescent spectra of the title complex were investigated at room temperature. In the solid state, the title complex exhibits multi-band emission centered

at 419, 433, and 468 nm. The first band at 419 nm is assigned to the own emission of separate [ZnL] species in excellent agreement with the theoretical prediction (412 nm for vertical transition). The shoulders at 433 and 468 nm correspond, in our opinion, to the two types of excimer emission (Figure 5).

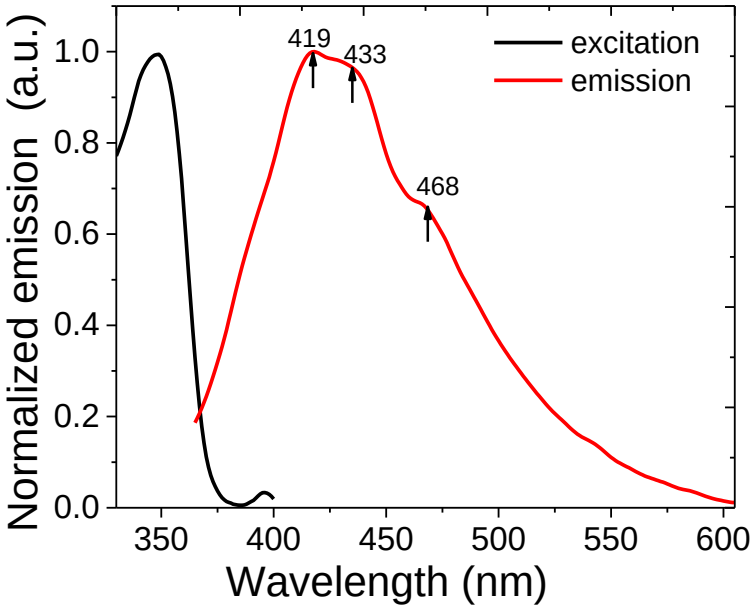

Figure 5. Solid-state excitation and emission spectra for the dispersed crystalline sample of [ZnL] complex.

Table 3. Photoluminescent properties of complex **1**

Parameter	CH_3CN	$CHCl_3$	EtOH	THF	Solid (cryst)
λ_{em} (λ_{ex}) (nm)	429 (343)	460 (372)	432 (352)	441 (365)	419, 433 (sh), 468 (sh)
τ (ns)	3.56	4.12	2.44	3.35	3.15
QY (%)	19	9.1	9.3	6.1	5.1

Our theoretical calculations clearly indicate that the band at 433 nm does not correspond to the vibronic satellite of the S_1-S_0 transition of the separate [ZnL] molecule because of negligibly small overlapping between the vibrational

wavefunctions of the final and initial states.[60,61] At the same time we have successfully optimized the structure of two excited state dimers (excimers) with the different degree of overlapping between the organic ligands. The excimer 1 (Figure 6) possesses the higher overlapping degree between the ligands comparing with the excimer 2. Due to this fact, excimer 1 demonstrates much strongly red-shifted emission at 468 nm (calc. 487 nm) comparing with the excimer 2 (434 nm vs calc. 433 nm) because of the stronger exchange interactions for excimer 1. As can be seen from Figure 6 both considered [ZnL] dimers are strongly unstable in the ground electronic state because of the destabilizing (non-bonding) nature of degenerated HOMO and HOMO-1 orbitals. The next HOMO-2 and HOMO-3 orbitals (Figure 6) slightly stabilize the dimers but not enough for the existence of the complexes in the ground electronic singlet state (S_0). At the same time, coupling between the LUMO wave functions of monomers strongly stabilizes both excimers 1 and 2. In fact, the population of LUMO orbital in the first excited singlet state (S_1) provides the higher stabilization of the dimer than destabilization by HOMO orbital. That is why both complexes are stable in S1 state, but do not exist in the ground electronic state. The idea about two excimers at 433 and 468 nm is also proved by the biexponential behaviour of photoluminescence decay[62,63] measured at these emission maxima with the predominant contribution of long-lifetime component 15.9 ns (83%) and 22.5 ns (81%), respectively (Figure S3).

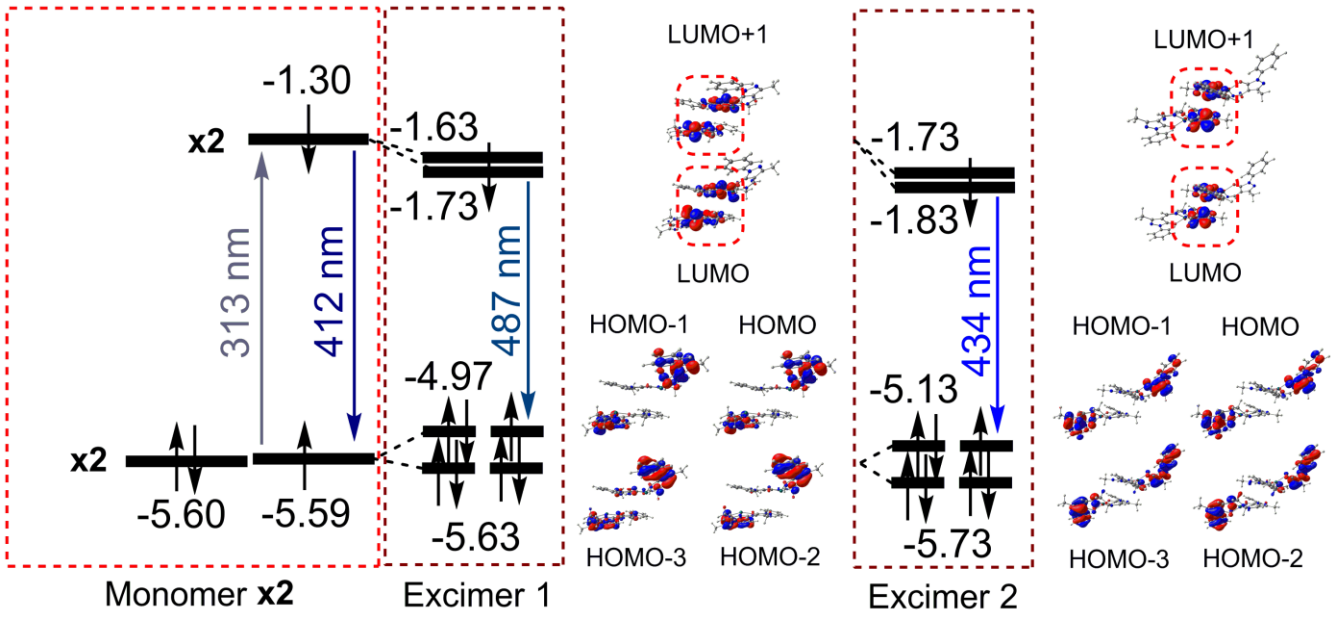

Figure 6. The scheme of excimer formation and emission for the [ZnL] species. The energy of orbitals is presented in eV. The absorption and emission wavelengths correspond to the vertical electronic transitions.

Crystalline sample demonstrates quite low luminescence efficiency (QY = 5.1 %), but unhydrated sample (obtained by boiling of hydrated samples in benzene) that demonstrates much more intense emission with quantum yield about 70.4%, which is obviously related with the removal of OH-oscillators from the coordination sphere.

5. DEVICE FABRICATION

To realize the potential of anhydrous [ZnL] complex as an emitter, it has been implemented in OLED structures. Two types OLED were fabricated based on the anhydrous [ZnL] complex with the following structures: ITO/TPD (40nm)/[ZnL] (20nm)/ PDB (40nm)/ Ca (20nm)/Al(150nm) (A) and ITO/TPD (40nm)/20%[ZnL]:mCP (20nm)/ PDB (40nm)/ Ca (20nm)/Al(150nm) (B). As an

electron-transporting and electron-injection 2-(4-biphenylyl)-5-phenyl-1,3,4-oxadiazole (PBD) layer and the hole transporting N,N′-Bis(3-methylphenyl)-N,N′-diphenylbenzidine (TPD) layer were incorporated into the device scheme. Since the Ca metal is highly reactive and corrodes quickly in the ambient atmosphere, the Ca layer topped with 150 nm aluminium (Al) layer was used as the cathode, while the ITO was used as anode material.

Typically, a doping system is often used in OLEDs in order to prevent concentration quenching and to improve device efficiency. Two types of OLEDs with different emitting layers (EML) have been fabricated with undoped and doped [ZnL] species in the 1,3-bis(N-carbazolyl)benzene (mCP) host.

The mCP has chosen as a host material due to good film-forming properties, carrier transporting characteristics and high thermal stability. Also, the emission (fluorescence) spectrum of the host material strongly overlaps with absorption spectrum of [ZnL] complexes (Figure S4) which is useful for efficient Förster resonance energy transfer (FRET). Actually, the efficiency of FRET reaches almost 100% upon the doping concentration of [ZnL] 10% and higher (20% for device B) that can be seen from Figure S5. The energy levels of the materials used in OLEDs A and B are displayed in Figure. 7.

In the EL spectrum of the single-layer and doped OLEDs (Figure 8) the emission bands of the neat zinc complex remain similar to the PL spectrum the crystalline sample including the excimer emission shoulder in the region of 480-490 nm. The excimer emission around 430 nm is absent in the EL spectrum of both devises. It is probably caused by the regular (homogeneous) structure and small thickness of the [ZnL] and

ZnL:mCP films upon thermovacuum deposition (Figure 7). It is important to note that excimer band at 485 nm becomes relatively weak in the EL spectrum of the ZnL/mCP doped OLED comparing with the undoped device; that is expected because of the decrease of excimer concentration in the ZnL:mCP blends.

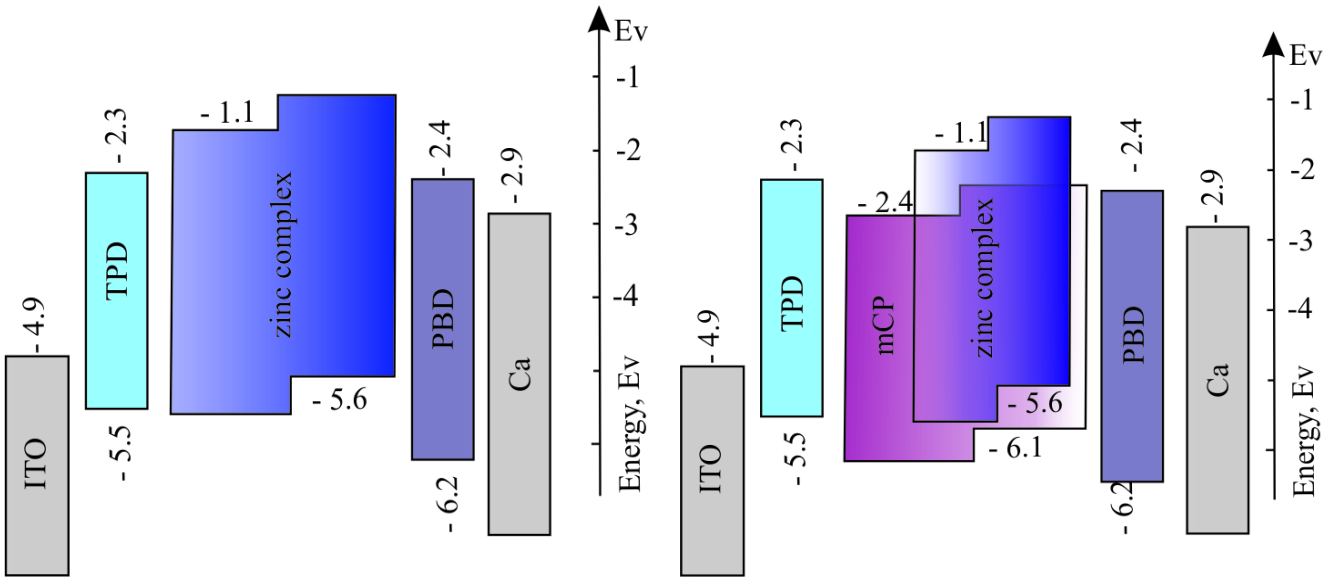

a *b*

Figure 7. Schematic energy diagram of devices 1 (a) and 2 (b)

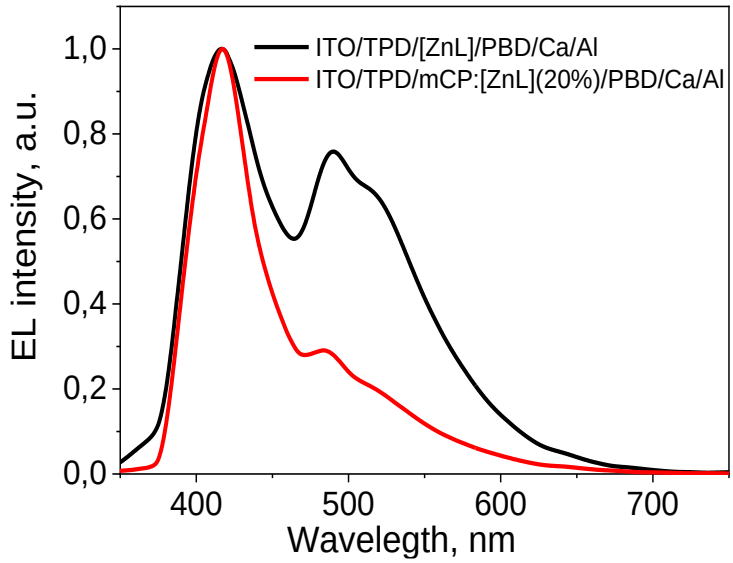

Figure 8. Electroluminescence spectra of undoped device A and doped device B.

A summarized output characteristics of OLEDs are shown in Table 4. The two types of OLEDs showed a similar blue emission. Color coordinates for devices A and B have been founded at (0.24; 0.27) and (0.22; 0.19) respectively (Figure 9). Figure 10 shows the current density-voltage characteristics, luminance-voltage characteristics (a) and external quantum efficiency (b) of the host-doped type device in comparison with the single-layer OLED.

Table 4. The lighting characteristics of the fabricated devices

Device	Max. brightness, cd/m^2	Max. current efficiency, cd/A	Max. power efficiency, lm/W	Max. EQE, %	Colour coordinate
OLED A	13 000(10V)	8.6	2.6	2.9	(0.24; 0.27)
OLED B	17 000(14V)	13.8	7.6	5.0	(0.22; 0.19)

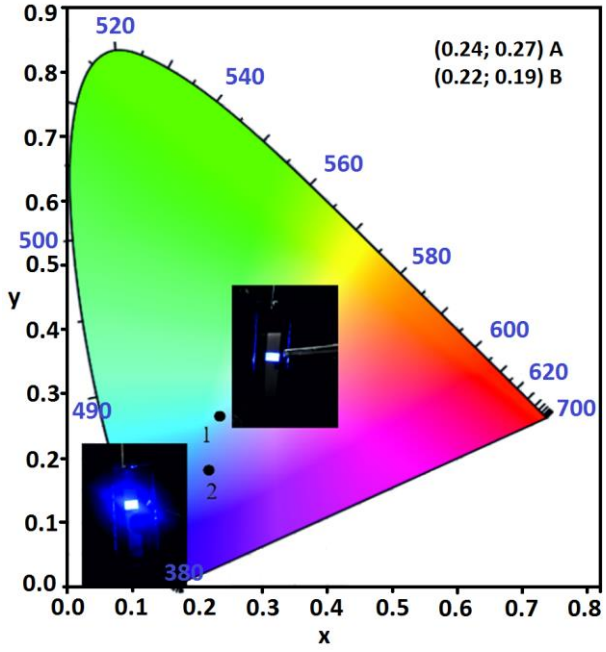

Figure 9. CIE1931 chromaticity coordinates including the position and photo of fabricated devices **A** and **B**.

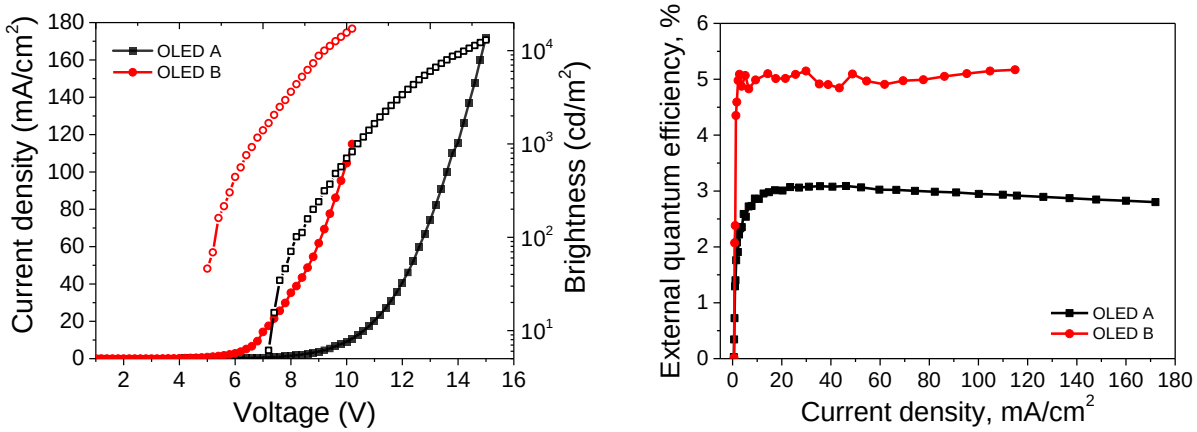

a *b*

Figure 10. Current density-voltage-brightness characteristics and current density-external quantum efficiency of the studied devices.

Undoped devices (OLED **A**) showed turn-on voltage at 7.5 V where at the same time doped device exhibited smaller turn-on voltage at 5V (at 10 cd/m^2). Devices **A** and **B** exhibited maximum brightness of 13 000 cd/m^2 (10V) and 17 000 cd/m^2 (14V) and maximum current efficiency were founded to be 8.6 cd/A and 13.8 cd/A, respectively. The doped OLED **B** demonstrates the maximum quantum efficiency close to 5%, what is behind of 2.9% EQE for undoped OLED **A**. Such observation can be explained more efficient exciton recombination process in the OLED B and host guest energy transfer. The efficient Förster energy transfer from the host mCP molecules to the molecules of [ZnL] emitter provided the considerable improving of lighting characteristics of device B comparing with undoped device A. One could say that the brightness and EQE parameters of the undoped device A is comparable with the state-of-art characteristics of related purely fluorescent (non-TADF) undoped blue OLEDs (Table 2 in Ref.[64]),

while the doped device **B** demonstrates an extraordinary brightness about 17 000 cd/m^2 comparing with other modern blue OLEDs.[10-17,65-67]

A possible way to improve the lighting parameters of the fabricated devices could be: 1) manipulating with the dopant concentration and host matrix material to reduce the excimer emission that should significantly decrease the value of the y coordinate on the CIE plot so that a deep blue narrow emission can be achieved to satisfy BT.2020 standard;[68] 2) manipulating with the thickness of functional layers to decrease the current density parameter and thus to enhance the current and power efficiency. Actually, the present paper demonstrates for the first time the utilization of an Zn azomethin-zinc complex as emissive material to construct really efficient high-luminance purely fluorescent blue OLEDs that many times surpasses the previously published analogues[69-71] (by one to two orders of magnitude for brightness, EQE, current and power efficiencies). Comparison between the lighting characteristics of the devices A and B, fabricated in this work with other previously published blue OLEDs based on the Schiff-base Zinc complexes is summarized in Table S5.

6. CONCLUSIONS

In the present work we have presented for the first time the synthesis and comprehensive structural, spectroscopic and theoretical characterization of the novel Zinc complex with N,N'-ethylamine-bis[1-phenyl-3-methyl-4-formylimino-2-pyrazoline-5-ol] ligand. This complex demonstrates deep blue fluorescence both in solution and solid state and was used for the fabrication of light-emitting devices (OLEDs). The electroluminescence spectra of the designed OLEDs contain a main band

of single-molecule fluorescence around 419 nm accompanied by two shoulders at 433 and 468 nm. Our experimental measurements and TDDFT calculations give evidence that these emission maxima correspond to the fluorescence of two different excimers that are characterized by different strengths of the stacking-interactions between the ligands of two neighboring complexes. The lighting characteristics of the fabricated OLEDs (maximum brightness of 17 000 cd/m^2 (14V), maximum current efficiency of 13.8 cd/A and external quantum efficiency close to 5% for the best device) are comparable with state-of-art results for the purely fluorescent (non-TADF) OLEDs.[65-67] Moreover, it is an absolute record among the wide family of Zinc complexes with Schiff bases (Table S5). The future improvement of chromaticity parameters for the studied devices by reducing of excimer shoulders might lead to cheap and efficient deep blue OLEDs with a large potential for industrial implementation.

SUPPORTING INFORMATION

The Supporting Information is available free of charge on the ACS Publications website at DOI: 10.1021/acs.jpcc.XXXXXXX. FTIR and excitation spectra, PL decay curves, emission spectra of mCP:[ZnL] films with different dopant concentration, overlapping area between mCP emission spectrum and [ZnL] absorption spectrum, results of theoretical assignment of FTIR, additional data from Bader's topological analysis and Cartesian coordinates for the $([ZnL]\cdot H_2O)_3$ fragment of crystal packing, comparison between the lighting characteristics of the devices A and B and other previously published blue OLEDs based on the Schiff-base Zinc complexes (PDF).

CORRESPONDING AUTHOR

*E-mail: galex0330@gmail.com

NOTES

The authors declare no competing financial interest.

ACKNOWLEDGEMENTS

Authors would like to acknowledge the financial support from the Ministry of education and science of Russian Federation (project № 10.1622.2017/PP), and Russian Science Foundation (project No. 17-73-20012). M.C. and G.W.S. are grateful for financial support from grant 674990 EXCILIGHT-H2020-MSCA-ITN-2015. M.A.K. is grateful for financial support from the State Assignment on Fundamental Research of the Kurnakov Institute of General and Inorganic Chemistry.

REFERENCES

[1] Eliseeva, S. V.; Bunzli J.-C. G. Lanthanide Luminescence for Functional Materials and Bio-Sciences. *Chem. Soc. Rev.*, **2010**, *39*, 189-227.

[2] Binnemans, K. Lanthanide-Based Luminescent Hybrid Materials. *Chem. Rev.*, **2009**, *109*, 4283-4374.

[3] Bettencourt-Dias, A. Lanthanide-Based Emitting Materials in Light-Emitting Diodes. *Dalton Trans.*, **2007**, 2229-2241.

[4] Schubert, E. F.; Kim, J. K. Solid-State Light Sources Getting Smart. *Science*, **2005**, *308*, 1274-1278.

[5] Feldmann, C.; Jüstel, T.; Ronda, C. R.; Schmidt, P. J. Inorganic Luminescent Materials: 100 Years of Research and Application. *Adv. Funct. Mater.*, **2003**, *13*, 511-516.

[6] Kim, S.; Bae, H. J.; Park, S.; Kim, W.; Kim, J.; Kim, J. S.; Jung, Y.; Sul, S.; Ihn, S.-G.; Noh, C., et al. Degradation of Blue-Phosphorescent Organic Light-Emitting Devices Involves Exciton-Induced Generation of Polaron Pair Within Emitting Layers. *Nat. Commun.*, **2018**, *9*, 1211.

[7] Seok, O. C.; Min, C. J.; Yeob, L. J. Chemical Bond Stabilization and Exciton Management by CN Modified Host Material for Improved Efficiency and Lifetime in Blue Phosphorescent Organic Light‐Emitting Diodes. *Adv. Opt. Mater.*, **2016**, *4*, 1281–1287.

[8] Murawski, C.; Leo, K.; Gather, M. C. Efficiency Roll‐Off in Organic Light‐Emitting Diodes. *Adv. Mater.*, **2013**, *25*, 6801-6827.

[9] Lee, H.; Lee, J.; Lee, J.-I.; Cho, N. S. Improvement of Colour Gamut in Bottom-Emission Organic Light-Emitting Diodes Using Micro-Cavity Structure Embedded Cathodes. *Electronics*, **2018**, *7*, 155.

[10] Chen, W.-C.; Yuan, Y.; Ni, S.-F.; Tong, Q.-X.; Wong, F.-L.; Lee, C.-S. Achieving Efficient Violet-Blue Electroluminescence With CIEy <0.06 and EQE >6% from Naphthyl-Linked Phenanthroimidazole–Carbazole Hybrid Fluorophores. *Chem. Sci.*, **2017**, *8*, 3599–3608.

[11] Chen, W.-C.; Yuan, Y.; Xiong, Y.; Rogach, A. L.; Tong, Q.-X.; Lee, C.-S. Aromatically C6- and C9-Substituted Phenanthro[9,10-d]imidazole Blue Fluorophores: Structure–Property Relationship and Electroluminescent Application. *ACS Appl. Mater. Interfaces*, **2017**, *9*, 26268–26278.

[12] Liu, B.; Zhu, Z.-L.; Zhao, J.-W.; He, D.; Wang, Z.-Y.; Luo, C.-Y.; Tong, Q.-X.; Lee, C.-S.; Tao, S.-L. Ternary Acceptor-Donor-Acceptor Asymmetrical Phenanthroimidazole Molecule for Highly Efficient Near- Ultraviolet Electroluminescence with External Quantum Efficiency (EQE) >4%. *Chem. Eur. J.*, **2018**, *24*, 15566–15571.

[13] Jayabharathi, J.; Ramya, R.; Thanikachalam, V.; Nethajia P. Tailoring the Molecular Design of Twisted Dihydrobenzodioxin Phenanthroimidazole Derivatives for Non-Doped Blue Organic Light-Emitting Devices. *RSC Adv.*, **2018**, *8*, 29031-29043.

[14] Liu, H.; Bai, Q.; Yao, L.; Zhang, H.; Xu, H.; Zhang, S.; Li, W.; Gao, Y.; Li, J.; Lu, P.; Wang, H.; Yang, B.; Ma, Y. Highly Efficient Near Ultraviolet Organic Light-Emitting Diode Based on a Meta-Linked Donor–Acceptor Molecule. *Chem. Sci.*, **2015**, *6*, 3797–3804.

[15] S. Zhang, L. Yao, Q. Peng, W. Li, Y. Pan, R. Xiao, Y. Gao, C. Gu, Z. Wang, P. Lu, F. Li, S. Su, B. Yang, Y. Ma, Achieving a Significantly Increased Efficiency in Nondoped Pure Blue Fluorescent OLED: A Quasi‐Equivalent Hybridized Excited State. *Adv. Funct. Mater.*, **2015**, *25*, 1755–1762.

[16] De, J.; Yang, W.-Y.; Bala, I.; Gupta, S. P.; Yadav, R. A. K.; Dubey, D. K.; Chowdhury, A.; Jou, J.-H.; Pal, S. K. Room-Temperature Columnar Liquid Crystals as Efficient Pure Deep-Blue Emitters in Organic Light-Emitting Diodes with an External Quantum Efficiency of 4.0%. *ACS Appl. Mater. Interfaces*, **2019**, *11*, 8291−8300.

[17] J. De, S. P. Gupta, S. S. Swayamprabha, D. K. Dubey, I. Bala, I. Sarkar, G. Dey, J.-H. Jou, S. Ghosh, S. K. Pal, Blue Luminescent Organic Light Emitting Diode Devices of a New Class of Star-Shaped Columnar Mesogens Exhibiting π−π Driven Supergelation. *J. Phys. Chem. C,* **2018**, *122*, 23659−23674.

[18] Tanaka, H.; Tokito, S.; Taga, Y.; Okada, A. Novel Metal–Chelate Emitting Materials Based on Polycyclic Aromatic Ligands for Electroluminescent Devices. *J. Mater. Chem.*, **1998**, *8*, 1999-2003.

[19] Wang, S. Luminescence and Electroluminescence of Al(III), B(III), Be(II) and Zn(II) Complexes with Nitrogen Donors. *Coord. Chem. Rev.*, **2001**, *215*, 79-98.

[20] Evans, R. C.; Douglas, P.; Winscom, C. J. Coordination Complexes Exhibiting Room-Temperature Phosphorescence: Evaluation of their Suitability as Triplet Emitters in Organic Light Emitting Diodes. *Coord. Chem. Rev.*, **2006**, *250*, 2093-2126.

[21] Xu, H.; Chen, R.; Sun, Q.; Lai, W.; Su, Q.; Huang W.; Liu, X. Recent Progress in Metal–Organic Complexes for Optoelectronic Applications. *Chem. Soc. Rev.*, **2014**, *43*, 3259-3302.

[22] Kotova, O. V.; Eliseeva, S. V.; Averjushkin, A. S.; Lepnev, L. S.; Vaschenko, A. A.; Rogachev, A. Yu.; Vitukhnovskii, A. G.; Kuzmina, N. P. Zinc(II) Complexes

with Schiff Bases Derived from Ethylenediamine and Salicylaldehyde: the Synthesis and Photoluminescent Properties. *Russ. Chem. Bull.*, **2008**, *57*, 1880-1889.

[23] Dumur, F.; Contal, E.; Wantz, G.; Gigmes, D. Photoluminescence of Zinc Complexes: Easily Tunable Optical Properties by Variation of the Bridge Between the Imido Groups of Schiff Base Ligands. *Eur. J. Inorg. Chem.*, **2014**, 4186-4189.

[24] La Deda, M.; Ghedini, M.; Aiello, I.; Grisolia, A. A New Blue Photoluminescent Salen-like Zinc Complex with Excellent Emission Quantum Yield. *Chem. Lett.*, **2004**, *33*, 1060-1061.

[25] Yu, G.; Liu, Y.; Song, Y.; Wua, X.; Zhu, D. A New Blue Light-Emitting Material. *Synth. Met.*, **2001**, *117*, 211-214.

[26] Zhang, G.; Yang, G.; Wang, S.; Chen, Q.; Ma, J. S. A Highly Fluorescent Anthracene‐Containing Hybrid Material Exhibiting Tunable Blue–Green Emission Based on the Formation of an Unusual "T‐Shaped" Excimer. *Chem. Eur. J.*, **2007**, *13*, 3630-3635.

[27] Lin, X.-J.; Shen, Z.; Xu, H.-J.; Li, Y.-Z.; Zhang, H.-T.; You, X.-Z. A Binuclear Tetrahedral Zinc(II) Complex of 2-(2-pyridyl)benzo[1,2-d;4,5-d′]diimidazole with Strong Blue Fluorescence. *Inorg. Chem. Commun.*, **2004**, *7*, 1167-1169.

[28] Dumur, F.; Beouch, L.; Tehfe, M.; Contal, E.; Lepeltier, M.; Wantz, G.; Graff, B.; Goubard, F.; Mayer, C. R.; Lalevée, J., et al. Low-Cost Zinc Complexes for White Organic Light-Emitting Devices. *Thin Solid Films*, **2014**, *564*, 351–360.

[29] Song, X.-Q.; Peng, Y.-Q.; Cheng, G.-Q.; Wang, X.-R.; Liu, P.-P.; Xu, W.-Y. Substituted Group-Directed Assembly of Zn(II) Coordination Complexes Based on Two New Structural Related Pyrazolone Based Salen Ligands: Syntheses, Structures and Fluorescence Properties. *Inorg. Chim. Acta*, **2015**, *427*, 13-21.

[30] Dong, X.-Y.; Gao, L.; Wang, F.; Zhang, Y.; Dong, W.-K. Tri- and Mono-Nuclear Zinc(II) Complexes Based on Half- and Mono-Salamo Chelating Ligands. *Crystals*, **2017**, *7*, 267.

[31] Kvitko, I. Ya.; Porai-Koshits, B. A. About the Structure of Hydrolysis Product of 1-Phenyl-3-methyl-4-dimethylaminmethylene-5-pyrazolone. *Zh. Org. Khim.*, **1964**, *34*, 3005-3013.

[32] Melhuish, W. H. J. Quantum Efficiencies of Fluorescence of Organic Substances: Effect of Solvent and Concentration of the Fluorescent Solute. *J. Phys. Chem.*, **1961**, *65*, 229-235.

[33] Demas, J. N.; Crosby, G. A. Measurement of Photoluminescence Quantum Yields. Review. *J. Phys. Chem.*, **1971**, *75*, 991-1024.

[34] Cherpak, V.; Stakhira, P.; Minaev, B.; Baryshnikov, G.; Stromylo, E.; Helzhynskyy, I.; Chapran, M.; Volyniuk, D.; Hotra, Z.; Dabuliene, A., et al. Mixing of Phosphorescent and Exciplex Emission in Efficient Organic Electroluminescent Devices. *ACS Appl. Mater. Interfaces*, **2015**, *7*, 1219-1225.

[35] Dolomanov, O.V.; Bourhis, L. J.; Gildea, R. J.; Howard, J. A. K.; Puschmann, H. OLEX2: A Complete Structure Solution, Refinement and Analysis Program. *J. Appl. Cryst.*, **2009**, *42*, 339-341.

[36] Sheldrick, G. M. SHELXT – Integrated Space-Group and Crystal-Structure Determination. *ActaCryst.*, **2015**, *A71*, 3-8.

[37] Becke, A. D. Density-Functional Thermochemistry. III. The Role of Exact Exchange. *J. Chem. Phys.*, **1993**, *98*, 5648-5652.

[38] Lee, C.; Yang, W.; Parr, R. G. Development of the Colle-Salvetti Correlation-Energy Formula into a Functional of the Electron Density. *Phys. Rev. B*, **1988**, *37*, 785-789.

[39] Frisch, M. J.; Pople, J. A.; Binkley, J. S. Self-Consistent Molecular Orbital Methods 25. Supplementary Functions for Gaussian Basis Sets. *J. Chem. Phys.*, **1984**, *80*, 3265-3269.

[40] Francl, M. M.; Pietro, W. J.; Hehre, W. J.; Binkley, J. S.; DeFrees, D. J.; Pople, J. A.; Gordon, M. S. Self-Consistent Molecular Orbital Methods. XXIII. A Polarization-Type Basis Set for Second-Row Elements. *J. Chem. Phys.*, **1982**, *77*, 3654-3665.

[41] Runge, E.; Gross, E. K. U. Density-Functional Theory for Time-Dependent Systems. *Phys. Rev. Lett.*, **1984**, *52*, 997-1000.

[42] Miertus, S.; Scrocco, E.; Tomasi, J. Electrostatic Interaction of a Solute with a Continuum. A Direct Utilizaion of Ab Initio Molecular Potentials for the Prevision of Solvent Effects. *Chem. Phys.*, **1981**, *55*, 117-129.

[43] Bader, R. F. W. *Atoms in Molecules. A Quantum Theory*, Clarendon Press, Oxford, **1990**. 438 p.

[44] Espinosa, E.; Molins, E.; Lecomte, C. Hydrogen Bond Strengths Revealed by Topological Analyses of Experimentally Observed Electron Densities. *Chem. Phys. Lett.*, **1998**, *285*, 170-173.

[45] Espinosa, E.; Alkorta, I.; Rozas, I. About the Evaluation of the Local Kinetic, Potential and Total Energy Densities in Closed-Shell Interactions. *Chem. Phys. Lett.*, **2001**, *336*, 457-461.

[46] Frisch, M. J.; Trucks, G. W.; Schlegel, H. B.; Scuseria, G. E.; Robb, M. A.; Cheeseman, J. R.; Scalmani, G.; Barone, V.; Petersson, G. A.; Nakatsuji, H., et al. *Gaussian 16, Revision A.03*, Gaussian, Inc., Wallingford CT, **2016**.

[47] Keith, T. A. *AIMAll (Version 10.07.25)*, TK Gristmill Software, Overland Park KS, USA, **2010**. <www.aim.tkgristmill.com>.

[48] Minaeva, V. A.; Minaev, B. F.; Baryshnikov, G. V.; Kopylova, T. N.; Gadirov, R. M.; Eremina, N. S. Study of Structure and Spectral Characteristics of the Binuclear Zinc Complex with (E)-2-({2-[3-(Pyridin-2-yl)-1H-1,2,4-triazol-5-yl]phenylimino}methyl)phenol. *Russ. J. Gen. Chem.*, **2011**, *81*, 2332-2344.

[49] Yang, L.; Powell, D. R.; Houser R. P. Structural Variation in Copper(I) Complexes with Pyridylmethylamide Ligands: Structural Analysis with a New Four-coordinate Geometry Index, τ_4. *Dalton Trans.*, **2007**, 955–964.

[50] Spackman, A. M. How Reliable Are Intermolecular Interaction Energies Estimated from Topological Analysis of Experimental Electron Densities? *Cryst. Growth. Des.*, **2015**, 15, 5624-5628.

[51] Vladimirova, K. G.; Freidzon, A. Ya.; Kotova, O. V.; Vaschenko, A. A.; Lepnev, L. S.; Bagatur'yants, A. A.; Vitukhnovskiy, A. G.; Stepanov, N. F.; Alfimov, M.

V. Theoretical Study of Structure and Electronic Absorption Spectra of Some Schiff Bases and Their Zinc Complexes. *Inorg. Chem.*, **2009**, *48*, 11123-11130.

[52] Koch, U.; Popelier, P. L. A. Characterization of C-H-O Hydrogen Bonds on the Basis of the Charge Density. *J. Phys. Chem.*, **1995**, *99*, 9747-9754.

[53] Baryshnikova, A. T.; Minaev, B. F.; Baryshnikov, G. V.; Sun, W.-H. Structure and Spectral and Luminescence Properties of the Trinuclear Zinc Complex with (E)-5-((2,6-Diethylphenylimino)methyl)-2-methylquinolin-8-ol: Experimental and DFT Study. *Russ. J. Inorg. Chem.*, **2015**, *60*, 1560-1567.

[54] Minaev, B. F.; Baryshnikov, G. V.; Korop, A. A.; Minaeva, V. A.; Kaplunov, M. G. Quantum-Chemical Investigation of the Structure and Electronic Absorption Spectra of Electroluminescent Zinc Complexes. *Opt. Spectrosc.*, **2013**, *114*, 30-40.

[55] Baryshnikov, G. V.; Minaev, B. F.; Korop, A. A.; Minaeva, V. A.; Gusev, A. N. Structure of Zinc Complexes with 3-(Pyridin-2-yl)-5-(arylideneiminophenyl)-1H-1,2,4-triazoles in Different Tautomeric Forms: DFT and QTAIM Study. *Russ. J. Inorg. Chem.*, **2013**, *58*, 928-934.

[56] Minaev, B. F.; Baryshnikov, G. V.; Korop, A. A.; Minaeva, V. A.; Kaplunov, M. G. Theoretical Investigation of the Structure and Electronic Absorption Spectrum of a Complex Zinc Bis-[8-(3,5-difluorophenylsulfanylamino)quinolinate]. *Opt. Spectrosc.* **2012**, *113*, 298-304.

[57] Valiev, R. R.; Telminov, E. N.; Solodova, T. A.; Ponyavina, E. N.; Gadirov, R. M.; Kaplunov, M. G.; Kopylova, T. N. Theoretical and Experimental

Investigation of Photophysical Properties of Zn(DFP SAMQ)$_2$. *Spectrochim Acta A Mol Biomol Spectrosc.* **2014**, *128*, 137-140.

[58] Baryshnikov, G.; Minaev, B.; Ågren, H. Theory and Calculation of the Phosphorescence Phenomenon. *Chem. Rev.*, **2017**, *117*, 6500-6537.

[59] Minaev, B. F.; Minaeva, V. A. MCSCF Response Calculations of the Excited States Properties of the O_2 Molecule and a Part of its Spectrum. *Phys. Chem. Chem. Phys.*, **2001**, *3*, 720-729.

[60] Karaush, N. N.; Valiev, R. R.; Baryshnikov, G. V.; Minaev, B. F.; Ågren, H. DFT Simulation of the Heteroannelated Octatetraenes Vibronic Spectra with the Franck–Condon and Herzberg–Teller Approaches Including Duschinsky Effect. *Chem. Phys.* **2015**, *459*, 65-71.

[61] Minaev, B. F.; Valiev, R. R.; Nikonova, E. N.; Gadirov, R. M.; Solodova, T. A.; Kopylova, T. N.; Tel'minov, E. N. Computational and Experimental Investigation of the Optical Properties of the Chromene Dyes. *J. Phys. Chem. A*, **2015**, *119*, 1948-1956.

[62] Baryshnikov, G. V.; Gawrys, P.; Ivaniuk, K.; Witulski, B.; Whitby, R. J.; Al-Muhammad, A.; Minaev, B.; Cherpak, V.; Stakhira, P.; Volyniuk, D., et al. Nine-Ring Angular Fused Biscarbazoloanthracene Displaying a Solid State Based Excimer Emission Suitable for OLED Application. *J. Mater. Chem. C*, **2016**, *4*, 5795-5805.

[63] Ivaniuk, K.; Cherpak, V.; Stakhira, P.; Hotra, Z.; Minaev, B.; Baryshnikov, G.; Stromylo, E.; Volyniuk, D.; Grazulevicius, J. V.; Lazauskas, A., et al. Highly Luminous Sky-Blue Organic Light-Emitting Diodes Based on the

Bis[(1,2)(5,6)]indoloanthracene Emissive Layer. *J. Phys. Chem. C*, **2016**, *120*, 6206-6217.

[64] Abdurahman, A.; Obolda, A.; Peng, Q.; Li, F. Efficient Deep Blue Fluorescent OLEDs with Ultra-Low Efficiency Roll-Off Based on 4H-1,2,4-Triazole Cored D-A and D-A-D Type Emitters. *Dyes Pigm.* **2018**, *153*, 10-17.

[65] Jung, H.; Kang, S.; Lee, H.; Yu, Y.-J.; Jeong, J. H.; Song, J.; Jeon, Y.; Park, J. High Efficiency and Long Lifetime of a Fluorescent Blue-Light Emitter Made of a Pyrene Core and Optimized Side Groups. *ACS Appl. Mater. Interfaces*, **2018**, *10*, 30022-30028.

[66] Heimel, P.; Mondal, A.; May, F.; Kowalsky, W.; Lennartz, C.; Andrienko, D.; Lovrincic, R. Unicolored Phosphor-Sensitized Fluorescence for Efficient and Stable Blue OLEDs. *Nat. Commun.* **2018**, *9*, 4990.

[67] Takita, Y.; Takeda, K.; Hashimoto, N.; Nomura, S.; Suzuki, T.; Nakashima, H.; Uesaka, S.; Seo, S.; Yamazaki, S. Highly Efficient Deep-Blue Fluorescent Dopant for Achieving Low-Power OLED Display Satisfying BT.2020 Chromaticity. *Journal of the SID*, **2018**, *26*, 55-63.

[68] ITU-R Recommendation BT.2020-2, "*Parameter Values for Ultra-High Definition Television Systems for Production and International Programme Exchange*" **2015**. 6 p.

[69] Nishal, V.; Singh, D.; Kumar, A.; Tanwar, V.; Singh, I.; Srivastava, R.; Kadyan, P. S. A New Zinc–Schiff Base Complex as an Electroluminescent Material. *J. Organ. Semiconduct.*, **2014**, *2*, 15-20.

[70] Lepnev, L.; Vaschenko, A.; Vitukhnovsky, A.; Eliseeva, S.; Kotova, O.; Kuzmina, N. OLEDs Based on Some Mixed-Ligand Terbium Carboxylates and Zinc Complexes with Tetradentate Schiff Bases: Mechanisms of Electroluminescence Degradation. *Synth. Metals*, **2009**, *159*, 625-631.

[71] Hamada, Y.; Sano, T.; Fujita, M.; Fujii, T.; Nishio, Y.; Shibata, K. Blue Electroluminescence in Thin Films of Azomethin-Zinc Complexes. *Jpn. J. Appl. Phys.*, **1993**, *32*, L511-L513.